

1 **Aerosol organic nitrogen across the global marine boundary**

2 **layer: distribution patterns and controlling factors**

3 Ningning Sun^{1,2}, Xu Yu^{2,3}, Jian Zhen Yu^{2,4*}, Bo Zhang¹, Yilan Li^{1,5}, Ye Hu¹, Zhe Li¹,

4 Zhenlou Chen¹, Guitao Shi^{1*}

5 ¹ Key Laboratory of Geographic Information Science (Ministry of Education), School
6 of Geographic Sciences and State Key Laboratory of Estuarine and Coastal Research,
7 East China Normal University, Shanghai, China

8 ² Division of Environment and Sustainability, Hong Kong University of Science &
9 Technology, Clear Water Bay, Kowloon, Hong Kong, China

10 ³ Jiangsu Key Laboratory of Atmospheric Environment Monitoring and Pollution
11 Control, Jiangsu Collaborative Innovation Center of Atmospheric Environment and
12 Equipment Technology, Joint International Research Laboratory of Climate and
13 Environment Change, School of Environmental Science and Engineering, Nanjing
14 University of Information Science and Technology, Nanjing, Jiangsu, China

15 ⁴ Department of Chemistry, Hong Kong University of Science & Technology, Clear
16 Water Bay, Kowloon, Hong Kong, China

17 ⁵ Department of Chemistry, State University of New York College of Environmental
18 Science and Forestry, Syracuse, NY, USA

19

20

21

22 *Correspondence:

23 Jian Zhen Yu (jian.yu@ust.hk)

24 Guitao Shi (gtshi@geo.ecnu.edu.cn)

25 **Abstract**

26 Organic nitrogen (ON) is an important yet poorly constrained component of aerosol
27 total nitrogen (TN), particularly over remote oceans. We quantified aerosol ON in 92
28 total suspended particulate samples collected across approximately 160° of latitude in
29 the marine atmospheric boundary layer (MABL) during Chinese Antarctic and Arctic
30 expeditions (2019–2024), using a newly developed method that simultaneously
31 determines ON and inorganic nitrogen. A significant latitudinal gradient was observed,
32 with significantly higher ON concentrations (expressed as N) in the Northern
33 Hemisphere ($83.3 \pm 141.4 \text{ ng m}^{-3}$) than in the Southern Hemisphere ($15.4 \pm 12.4 \text{ ng m}^{-3}$).
34 Regionally, coastal East Asia recorded the highest ON levels ($164.6 \pm 179.1 \text{ ng m}^{-3}$)
35 but a lower ON/TN ratio ($21.1 \pm 7.9\%$), indicating strong terrestrial and anthropogenic
36 influence. In contrast, the Arctic Ocean had lower ON concentrations ($19.1 \pm 19.0 \text{ ng}$
37 m^{-3}) but the highest ON/TN ratio ($38.6 \pm 12.4\%$), suggesting dominant marine biogenic
38 sources. The Southern Ocean showed the lowest ON concentration ($12.0 \pm 7.1 \text{ ng m}^{-3}$)
39 yet a relatively high ON/TN ratio ($27.8 \pm 11.0\%$), also pointing to oceanic origins.
40 Near Antarctica, samples influenced by sea-ice air masses displayed markedly
41 elevated ON and ON/TN ratios. These increases were strongly correlated with sea ice
42 concentration and chlorophyll-a exposure, indicating enhanced biogenic emissions
43 from sea-ice-associated ecosystems. This study offers the first direct ON
44 measurements along a global MABL transect, revealing distinct latitudinal and
45 regional patterns, and emphasizing the combined roles of continental inputs and
46 marine sources. It also identifies sea-ice dynamics as a key factor influencing ON in
47 Antarctic regions, providing crucial data for improving atmospheric and climate
48 models.

49

50 **Key points.**

51 1. Aerosol organic nitrogen (ON) in the global marine boundary layer was quantified
52 along a transect from the Antarctic to the Arctic (~160° latitude) for the first time.

53 2. A strong latitudinal gradient in ON was observed, revealing distinct hemispheric
54 and regional patterns.

55 3. Near Antarctic, ON concentrations and ON/TN ratios were distinctly elevated in
56 sea-ice-influenced air masses, highlighting the role of sea-ice-associated ecosystems | 删
57 as a likely driver of enhanced ON production and emissions.

58 **1. Introduction**

59 Marine atmospheric boundary layer (MABL) aerosol particles contain significant
60 amounts of organic nitrogen (ON) and inorganic nitrogen (IN), both recognized as
61 major components of atmospheric particulate matter (Li et al., 2023). ON may
62 account for roughly 20–80% of total reactive nitrogen deposition to the surface ocean,
63 implying a potentially large, yet uncertain, role in marine nitrogen cycling and climate
64 (Altieri et al., 2016, 2021). ON affects climate and biogeochemistry by supplying
65 bioavailable nitrogen, modifying cloud condensation nuclei and ice-nucleating
66 particle populations, and contributing to aerosol light absorption. Hygroscopic ON
67 compounds (e.g., amino acids, amines, sugars) enhance water uptake and cloud
68 condensation nuclei (CCN) activity; some proteinaceous organics act as efficient ice
69 nuclei (Alsante et al., 2024; Chan et al., 2005). Marine alkylamines can form salts
70 with sulfuric acid, promoting new particle formation and growth, thereby linking ON
71 to aerosol number and radiative forcing (Almeida et al., 2013; Brean et al., 2021).
72 Nitrogen-containing chromophores (brown nitrogen) can dominate the absorptive
73 properties of organic aerosol regionally and contribute substantially to global
74 absorption by carbonaceous aerosol (Li et al., 2025).

75 However, ON remains poorly constrained due to analytical limitations (Baker et
76 al., 2017). Previous studies focused on the water-soluble fraction of aerosol ON
77 (WSON) inferred indirectly by subtraction IN from total nitrogen (TN) (ON = TN –
78 IN), while the water-insoluble organic nitrogen (WION) fraction has been largely

79 unquantified (Cornell, 1999; Mace et al., 2003). The subtraction approach is prone to
80 errors and artifacts, especially when TN and IN concentrations are similar, leading to
81 underestimation and large uncertainties in ON burdens and fluxes. A novel method
82 developed by Yu et al. (2021) addresses these limitations. Based on thermal evolution
83 and chemiluminescence detection, this approach measures aerosol IN and ON
84 simultaneously, eliminating subtraction-based biases and capturing both WSON and
85 WION.

86 Aerosol ON arises from diverse sources. Marine pathways include primary
87 emissions via sea spray enriched with organic matter from the sea surface microlayer
88 and secondary formation from marine precursors (e.g., alkylamines) reacting with
89 acidic species (Facchini et al., 2008; Miyazaki et al., 2011a). Continental pathways
90 include long-range transport of organic emissions from fossil fuel combustion,
91 biomass burning, soils, and vegetation (Cape et al., 2011; Jickells et al., 2013; Luo et
92 al., 2018). Primary marine emissions inject large amounts of particulate matter
93 annually, carrying organic carbon and nitrogen from plankton, bacteria, and surface
94 films (Violaki et al., 2015a). Observations have shown that sea spray can carry
95 substantial ON and that WION can dominate ocean-influenced aerosol ON (Miyazaki
96 et al., 2011a).

97 While marine aerosol ON has been the subject of several studies, its sources in
98 remote oceanic regions remain a matter of debate. Some studies implicate continental
99 transport (e.g., dust, anthropogenic emissions), whereas others point to direct sea
100 spray emissions or secondary formation from marine-derived alkylamines (Altieri et
101 al., 2016; Lesworth et al., 2010; Zamora et al., 2011). Correlations between ON and
102 ocean biological proxies (e.g., chlorophyll-a) suggest in situ marine production,
103 particularly during phytoplankton blooms (Altieri et al., 2016; Dall’Osto et al., 2019).
104 Yet open-ocean and polar regions, where sea ice variability can strongly modulate
105 primary productivity and thus potentially influence ON emissions, remain sparsely
106 observed, limiting constraints on potential sea ice linked controls on ON, especially
107 for high latitudes (Altieri et al., 2016; Matsumoto et al., 2022). Around Antarctica in
108 particular, the paucity of direct ON measurements—especially of WION—limits

109 understanding of ON sources, seasonality, and impacts on high-latitude atmospheric
110 chemistry.

111 To address these gaps, we measured aerosol ON and IN using samples collected
112 during ~~four Chinese Arctic and Antarctic research expedition~~ campaigns, spanning
113 $\sim 160^\circ$ of latitude from the Arctic to Antarctica. The dataset, determined by this newly
114 developed analyzer, enables evaluation of hemispheric and regional patterns,
115 assessment of controlling factors (e.g., continental influence, marine biological
116 activity), and explicit investigation of sea-ice-associated processes near Antarctica.
117 The results provide observational constraints that can be used to refine the
118 representation of nitrogen cycling and atmosphere–ocean interactions in climate and
119 atmospheric chemistry models.

删除: three

删除: s

删除: We employed a newly developed aerosol nitrogen analyzer based on thermal evolution and chemiluminescence detection to measure aerosol IN and ON simultaneously, eliminating subtraction-based method biases and capturing both WSON and WION (Yu et al., 2021).

删除: improve

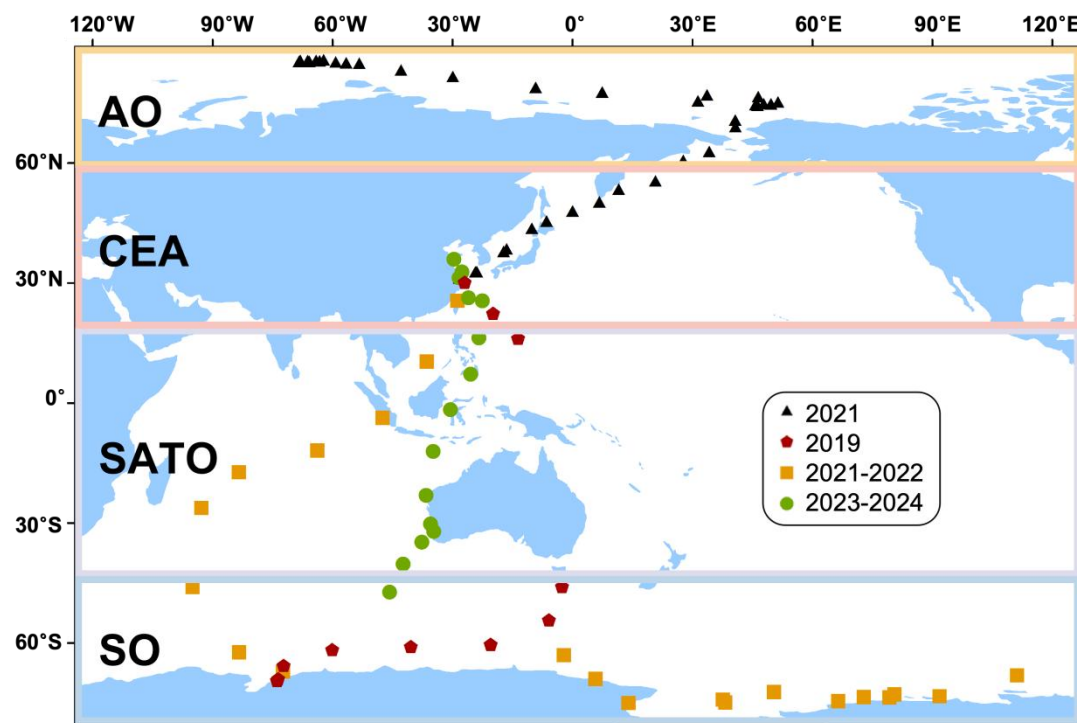
120 **2. Methodology**

121 **2.1. Sample Collection**

122 A total of 92 total suspended particulate (TSP) samples were collected during three
123 Chinese Antarctic research expeditions and one Arctic expedition aboard the
124 icebreaker R/V *Xuelong*. Sampling spanned a latitudinal range of approximately 160°
125 (86°N to 75°S), encompassing polar and mid-latitude marine regions. The Antarctic
126 samplings were conducted in October to November in 2019 (SP2019, 14 samples),
127 November 2021 to March 2022 (SP2021, 23 samples), and October 2023 to April
128 2024 (SP2023, 15 samples), while the Arctic campaign occurred in July to September
129 in 2021 (40 samples).

130 During the Antarctic campaigns, aerosols were collected using a high-volume air
131 sampler (HVAS, TISCH Environmental, USA; flow rate: $1.2 \text{ m}^3 \text{ min}^{-1}$) equipped with
132 pre-baked (500°C , 24 h) Whatman quartz filters ($20.3 \times 25.4 \text{ cm}$; Whatman Ltd., UK).
133 For Arctic sampling, a DIGITEL DHA-80 sampler (flow rate: 500 L min^{-1}) with 14.2
134 cm diameter Whatman quartz filters were employed. Each sample represented a 48 h
135 integrated collection period, corresponding to $2\text{--}4^\circ$ latitude traversed during ship
136 transits. To minimize contamination from ship emissions, a wind sector controller
137 restricted sampling to air masses within 120° of the ship's heading. Filters were

138 handled using nitrile gloves and masks to avoid potential contamination.
139 Post-sampling, filters were folded with the collection surface inward, wrapped in
140 pre-cleaned aluminum foil, sealed in polyethylene bags, labeled with sampling time
141 and location, and stored at -20°C. Detailed protocols followed established
142 methodologies (Shi et al., 2021). Following expeditions, samples were transported to
143 the laboratory under frozen conditions and maintained at -20°C until analysis. The
144 sampling location for the Antarctic and Arctic campaigns are illustrated in Fig. 1.



145
146 Figure 1. Total suspended particulate (TSP) aerosol sampling locations along the cruises path
147 from Shanghai, China to Antarctica and Arctic.

148 **2.2. Chemistry Analysis for major ions, EC and OC**

149 Major ions were quantified through ion chromatographic analysis of water extracts of
150 the aerosol samples. The extraction of filters in the laboratory followed protocols
151 comparable to those described in the previous study (Shi et al., 2021). Prior to
152 measurement, three-quarters of each filter was sectioned into small pieces using
153 acid-cleaned Teflon-coated scissors and transferred into high-purity Milli-Q water
154 (18.2 MΩ). The suspensions were subjected to ultrasonic treatment for 30 min,
155 followed by continuous shaking at 120 rpm for 12 h to ensure thorough extraction of

156 water-soluble components. The extracts were subsequently filtered through 0.22 μm
157 polytetrafluoroethylene (PTFE) membranes prior to ion analysis. The concentrations
158 of the main ions (NO_3^- , SO_4^{2-} , Na^+ , NH_4^+ , K^+ , and Ca^{2+}) in the sample were
159 determined by an ion chromatograph (AQ1100, RFIC, equipped with a CS12 column
160 (2 \times 250 mm) for cation analysis, AS11 column (2 \times 250 mm) for anion analysis,
161 Thermo Scientific, USA), and the eluents of cation and anion were 18.00 mM
162 methylsulfonic acid (MSA) and potassium hydroxide (KOH), respectively. During
163 sample analysis, the relative deviation of repeated assays ($n = 5$) of all ions is usually
164 less than 5%. We used the following formula to calculate non-sea salt SO_4^{2-}
165 (nss SO_4^{2-}), non-sea salt Ca^{2+} (nss Ca^{2+}) and non-sea salt K^+ (nss K^+):

$$[\text{nssSO}_4^{2-}] = [\text{total SO}_4^{2-}] - 0.253 \times [\text{Na}^+] \quad (1)$$

$$[\text{nssCa}^{2+}] = [\text{total Ca}^{2+}] - 0.038 \times [\text{Na}^+] \quad (2)$$

$$[\text{nssK}^+] = [\text{total K}^+] - 0.037 \times [\text{Na}^+] \quad (3)$$

166 where 0.252, 0.037, and 0.038 in the above expressions are the ratios of $\text{SO}_4^{2-}/\text{Na}^+$
167 (Quinby-Hunt and Turehian, 1983), $\text{Ca}^{2+}/\text{Na}^+$ (Anonymous, 1997), and K^+/Na^+ (Keene
168 et al., 1986) in the sea water, respectively.

169 OC and EC concentrations were determined using a Thermal/Optical Carbon
170 Analyzer (DRI, Model 2001, Atmoslytic Inc., USA) following the IMPROVE
171 protocol as implemented by Wu et al., (2024). OC and EC measurements were
172 conducted for aerosol filters collected during the 2021 Arctic and 2019 Antarctic
173 cruises.

174 **2.3. ON measurement**

175 Aerosol ON and IN were simultaneously measured using the recently developed
176 Aerosol Nitrogen Analyzer system, which enables sensitive quantification directly
177 from filter samples without pretreatment. Detailed descriptions of the method are
178 provided in Yu et al (2021). Briefly, the method detection limit is 96 ng N. Because
179 the detection limit scales inversely with the analyzed filter area, it can be readily
180 lowered by analyzing a larger aliquot. In this study, 4–6 cm² of filter material was
181 typically analyzed for each sample, yielding a proportionally lower effective detection

182 limit and ensuring stable and reliable quantification for low-concentration marine
183 aerosol samples. Compared with traditional IC-based approaches, this analyzer
184 provides a clear advantage by determining IN and ON simultaneously on the same
185 filter aliquot, thereby avoiding the subtraction-based “difference method” (ON = TN -
186 IN) and the associated uncertainty propagation when TN and IN are similar in
187 magnitude.

188 The analyzer integrates a thermal aerosol carbon analyzer and a
189 chemiluminescence NO_x analyzer. Aerosol samples collected on quartz fiber filters
190 were thermally evolved under a programmed 6-step temperature protocol (150, 180,
191 300, 400, 500, and 800 °C) in a 1% O₂/99% He carrier gas. The evolved materials
192 were catalytically oxidized to CO₂ and nitrogen oxides (NO_y), with the C signal
193 monitored via methanator-FID detection and the N signal recorded through
194 chemiluminescence after converting NO_y to NO. The C signal assists in
195 differentiating IN and ON components, as ON aerosols produce both C and N signals
196 while the IN fraction only yields an N signal. The programmed thermal evolution
197 facilitates separation of aerosol IN and ON due to their distinct thermal characteristics.

198 Specifically, IN and ON discrimination is achieved by jointly interpreting the C and N
199 thermograms: ON is identified by co-evolving C and N signals across the temperature
200 steps, whereas IN is characterized by N-only evolution without a corresponding C
201 signal. The separation of overlapping thermal features is further resolved using
202 multivariate curve resolution (MCR), which deconvolves the mixed thermograms into
203 source-like components based on their distinct thermal evolution patterns.

204 Quantification of IN and ON is achieved through multivariate curve resolution (MCR)
205 data treatment of the C and N thermograms using USEPA PMF (version 5.0).

206 **2.4. Backward Trajectory Analysis**

207 To study air mass origins, air mass backward trajectories have been calculated using
208 the Hybrid Single-Particle Lagrangian Integrated Trajectories (HYSPLIT) model with
209 meteorological fields from the National Oceanic and Atmospheric Administration
210 (NOAA) air resources laboratory GDAS database. Five-day backward trajectories

刪除: In brief, t

were calculated in order to reveal the history of the air masses arriving at the sampling site (Stein et al., 2015). Each trajectory originated at the vessel's real-time position with an arrival height of 20 m, capturing boundary layer transport while minimizing local ship influence. Air mass backward trajectories were simulated using the HYSPLIT model with meteorological fields from the NOAA GDAS database to reveal the transport history of air masses arriving at the vessel (Stein et al., 2015). Given that the ship was continuously moving and each sample integrates air masses over approximately 2–4 degrees of latitude, we applied a nested strategy to account for spatiotemporal variability. For the initial characterization of the entire dataset, a representative sampling location was defined for each sample using the average latitude and longitude of its start and end positions, with backward trajectories simulated at 6 h intervals anchored to this midpoint to identify dominant air-mass categories (Fig. 3). Subsequently, to precisely investigate the influence of sea ice on ON in the Southern Ocean and Antarctic marginal regions (Section 4.2), a targeted high-resolution analysis was performed on this subset of samples. For each Antarctic sample, the actual cruise track was equally divided into 48 points corresponding to the hourly intervals of the 48 h sampling period, and a 120 h backward trajectory was calculated for each of these 48 coordinates (Fig. S3a and b).

To determine whether the backward trajectories of the MABL samples were mainly influenced by the open ocean, sea-ice-covered regions, or the continental area, we calculated the time-weighted residence-time ratios of air masses over sea ice (R_S), open ocean (R_O), and the continental area (R_C) using the following equation:

$$R_S(R_O \text{ or } R_C) = \frac{\sum_{i=1}^{N_S(N_O \text{ or } N_C)} x e^{-(\frac{t_i}{120})}}{\sum_{i=1}^{N_{\text{total}}} x e^{-(\frac{t_i}{120})}} \quad (4)$$

where N_{total} denotes the total number of trajectory endpoints; N_S N_O and N_C represent the numbers of endpoints located over sea ice, the open ocean, and the Antarctic ice sheet, respectively. t_i is the backward-trajectory time (in hours), and $t_i/120$ is a time-weighting factor (Zhou et al., 2021). This factor accounts for air-mass dispersion during transport and aerosol removal by particle deposition; therefore, regions

238 associated with longer trajectory times exert weaker influences on the sampling site,
239 whereas nearby regions exert stronger influences. Accordingly, higher values of R_s
240 R_o and R_c indicate greater influences from sea ice, the open ocean, and the Antarctic
241 ice sheet, respectively.

242 2.5. Potential Source Contribution Function (PSCF) analysis

243 Potential Source Contribution Function (PSCF) analysis was implemented to identify
244 source regions of ON observed during the sampling period (Ashbaugh et al., 1985). A
245 higher PSCF value indicates a greater potential source contribution to the receptor site.
246 In our study, the PSCF domain was established within a grid cell encompassing all
247 backward trajectories. The cruises were discretized into 1° latitude \times 1° longitude grid
248 cells. The PSCF value for cell ij was calculated as:

$$249 PSCF_{ij} = \frac{\sum m_{ij}}{\sum n_{ij}} \quad (5)$$

250 where, m_{ij} = total trajectory endpoints within cell ij ; n_{ij} = subset of endpoints
251 associated with aerosol component concentrations exceeding the 75th percentile of
252 cruise measurements. To mitigate uncertainty in cells with sparse trajectory density, a
253 latitude-dependent weighting function (W) was applied:

$$254 W = \begin{cases} 1.0 & \text{when } n_{ij} > N2 \\ 0.8 & \text{when } N1 < n_{ij} < N2 \\ 0 & \text{when } n_{ij} < N1 \end{cases} \quad (6)$$

255 where n_{ij} is the number of trajectories passing for each cell in the study period and
256 $N1 = 60 * \cos(\text{latitude})$, and $N2 = 300 * \cos(\text{latitude})$. The cosine factor is used to
257 account for the changing grid cell size with varying latitude.

258 2.6. Air-mass exposure to chlorophyll a

259 The Air-mass Exposure to Chlorophyll a (Chl-a) index (AEC) serves as a quantitative
260 metric to assess the influence of marine biogenic emissions on a target region through
261 air mass transport (Blazina et al., 2017; Choi et al., 2019). This approach is grounded
262 in the well-established correlation between ocean surface phytoplankton biomass and
263 marine biogenic emissions, particularly dimethyl sulfide (DMS), where Chl-a
264 concentration acts as a robust proxy for phytoplankton abundance (Siegel et al., 2013).

删除:

Probability Source Contribution Function analysis

删除: 4

删除: 5

265 The AEC index estimates the integrated exposure of an air mass to oceanic DMS
266 source regions along its trajectory by accounting for both spatial distribution of Chl-a
267 and atmospheric vertical mixing dynamics (Zhou et al., 2023).

268 For each trajectory point, Chl-a concentrations (Chl_{ai}) were obtained from
269 satellite remote sensing products (Aqua-MODIS, OCI algorithm; 8-day composite, 4
270 km \times 4 km resolution; <https://oceancolor.gsfc.nasa.gov/l3/>) within a 20 km radius to
271 reduce the influence of missing/cloud-contaminated pixels and pixel-scale noise,
272 while remaining small enough to preserve local marine biological variability relevant
273 to each trajectory point. The 20 km radius approach has been widely adopted in
274 previous studies to mitigate the uncertainty of trajectory endpoints and ensure robust
275 matching with satellite data coverage in previous research (Park et al., 2018; Zhou et
276 al., 2021, 2023). Trajectory endpoints over Antarctica, sea-ice-covered areas, or at
277 pressures < 850 hPa were assigned Chl-a = 0 because air masses at these altitudes are
278 generally decoupled from local ocean surface biological activity (Zhou et al., 2023).

279 Points without valid Chl-a data were excluded. The AEC for a single trajectory was
280 computed as:

$$281 \quad \text{AEC} = \frac{\sum_{i=1}^{120} \text{Chl}_{ai} \times e^{-\frac{t_i}{120}}}{n} \quad (7)$$

282 where t_i denotes time backward along the trajectory (hours), and n is the total number
283 of valid trajectory points. The time points when the air mass passed over the continent
284 or regions covered by sea ice were assigned a zero chlorophyll value. To ensure
285 robustness, trajectories with $n < 90$ (75% of 120 h data points at hourly resolution)
286 were discarded. For each sample, the final AEC value was derived from the arithmetic
287 mean of all valid trajectories during the sampling period (Yan et al., 2024).

288 2.7. Sea ice concentration

289 In this study, remote sensing data are utilized to illustrate the spatiotemporal
290 distribution of sea ice concentrations (SICs) in the Southern Ocean. For regional-scale
291 visualization of sea-ice extent (SIE) and SIC variability, we used the Sea Ice Index
292 (Version 3) distributed by the National Snow and Ice Data Center (NSIDC) (Fetterer

293 et al., 2017), which is derived from passive-microwave observations from DMSP
294 SSM/I and SSMIS sensors (Cavalieri et al., 1997).

295 Sea-ice concentrations used here are derived from daily gridded
296 passive-microwave SIC products, which provide all-weather coverage and are widely
297 used for polar sea-ice monitoring. The SIC of each sample is calculated using the
298 following formula:

299
$$SIC = \frac{\sum_{i=1}^{Ns} SIC_i}{Ns} \quad (8)$$

删除: 7

300 where SIC_i represents the average sea ice density at the endpoint of the specified track.
301 Ns represents the total number of trajectory endpoints located on the sea ice area. For
302 each trajectory endpoint, the SIC value was extracted by collocating the endpoint
303 latitude/longitude and the corresponding day with the daily SIC grid; the SIC_i for each
304 sample was then calculated as the mean SIC across all sea-ice-covered endpoints (Ns).

305 Sea ice concentration data are from the AMSR2 dataset (Version 5.4. University of
306 Bremen, Germany. Index of /amsr2/asi_daygrid_swath/s3125).

307 3. Results

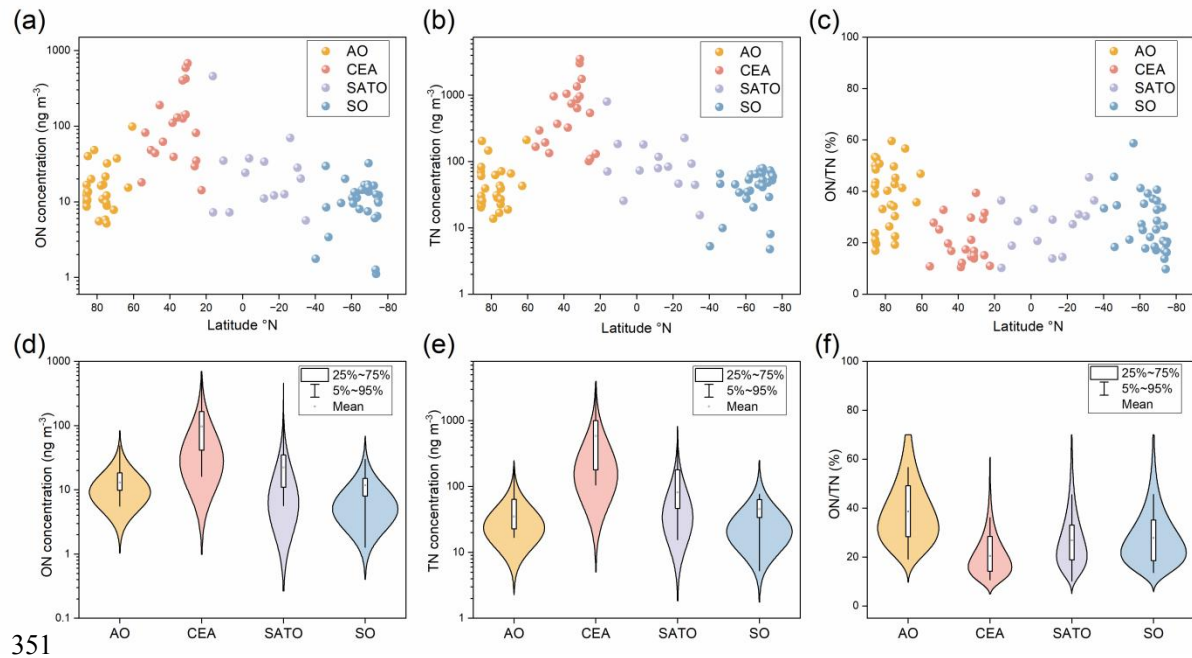
308 Atmospheric ON concentrations (expressed as N, the same hereafter) exhibited
309 significant hemispheric differences ($p < 0.001$; Mann–Whitney U test; Table S1), with
310 values in the Northern Hemisphere (NH: $83.3 \pm 141.4 \text{ ng m}^{-3}$, $N = 55$) being
311 approximately five times higher than those in the Southern Hemisphere (SH: $15.4 \pm$
312 12.4 ng m^{-3} , $N = 37$). The ON/TN ratios showed broadly similar magnitudes between
313 hemispheres, with slightly higher in the NH ($30.4 \pm 13.6\%$) compared to the SH (27.9
314 $\pm 10.6\%$). Samples from three Antarctic cruises—SP2019 (mean = 19.4 ng m^{-3} ; range:
315 $9.5\text{--}555.6 \text{ ng m}^{-3}$), SP2021 (mean = 20.4 ng m^{-3} ; range: $1.3\text{--}81.3 \text{ ng m}^{-3}$), and
316 SP2023 (mean = 18.3 ng m^{-3} ; range: $1.8\text{--}457.0 \text{ ng m}^{-3}$) showed no significant
317 variation (one-way ANOVA; $p > 0.2$), indicating that interannual variation was rather
318 minor. A clear latitudinal gradient in ON concentrations was observed along the
319 Antarctic-to-Arctic transect, with peak values in the $20\text{--}40^\circ \text{ N}$ zone and a gradual
320 decline toward both polar regions (Fig. 2a). Based on spatial distribution patterns, the
321 study transect can be divided into four regions (Fig. 1): (1) the Arctic Ocean region

删除: independent samples t-test;

322 (AO, north of \sim 60° N); (2) the Coastal East Asia region (CEA, 20–60° N); (3) the
323 Southeast Asia-Australia Tropical Ocean region (SATO, \sim 20° N–40° S); and (4) the
324 Southern Ocean region (SO, south of \sim 40° S).

325 The CEA region exhibited the highest ON concentrations (mean = 164.6 ng m⁻³)
326 but the lowest ON/TN ratio (mean = 21.1, ~~± 7.9%~~). In contrast, the SO region showed | 删除: %
327 the lowest ON concentrations (mean = 12.0 ng m⁻³; range: 1.8–32.3 ng m⁻³) and
328 higher ON/TN ratios (mean = 27.8, ~~± 11.0%~~). Notably, the AO region displayed the | 删除: %
329 highest ON/TN ratios (mean = 38.6, ~~± 12.4%~~) despite relatively low ON | 删除: %
330 concentrations (mean = 19.1 ng m⁻³; range: 5.2–32.2 ng m⁻³). The ON/TN ratio in
331 SATO region (26.8, ~~± 10.0%~~) is similar to that of SO but with a lower ON | 删除: %
332 concentration (mean = 23.4 ng m⁻³; range: 5.7–70.1 ng m⁻³), which is much lower
333 than the CEA region, but higher than the high latitude two pole regions.

334 Since direct measurement data of total ON in global MABL are limited, WSON
335 data were summarized for comparison (Table 1). Overall, the previous results are
336 consistent with the spatial trends of ON in our study. WSON concentrations exhibit
337 significant spatial variation, generally higher in the NH than in the SH, highlighting
338 the substantial contribution of anthropogenic sources (Violaki et al., 2015b). In
339 addition, WSON concentrations tend to be higher closer to land, while in remote
340 ocean areas, WSON levels are generally lower. The reported ratios of WSON/~~WSTN~~
341 in previous studies vary significantly across different investigation sites. Moreover, in
342 remote marine environments, the WSON/~~WSTN~~ ratio is relatively high, suggesting
343 that WSON plays a substantial role in the biogeochemical cycle of nitrogen within
344 these remote regions. It is important to note that most previous studies over the
345 remote ocean measured only WSON, without accounting for the WION. As a result,
346 the ON/TN ratios in this region were likely underestimated. Based on our comparison,
347 the total ON concentration in the Southern Ocean may have been underestimated by
348 approximately 40%, hinting the significant contribution of the insoluble organic
349 fraction that has been largely overlooked in earlier datasets due to measurement
350 method limitations.



351

352 Figure 2. Latitudinal distributions of ON concentration, TN concentration and ON/TN ratio (a, b,
 353 c), and the statistics (d, e, f) over the the Arctic Ocean region (AO), the Coastal East Asia region
 354 (CEA), the Southeast Asia-Australia Tropical Ocean region (SATO) and the Southern Ocean
 355 region (SO), respectively.

Table 1. Measured concentrations of WSON from published reports in the marine atmospheric boundary layer.

Regions	Period	Locations	WSON (ng m ⁻³)	Ratio to <u>WSTN</u> (%)	Methods for IN	Methods for <u>WSTN</u>	Reference
Southern Atlantic	2007.01-02	35° S-45° S	119 ± 163.8	-	IC	PO	(Violaki et al., 2015b)
the Northwest Pacific Ocean	2014.2015	25–40° N, 125–150° E	43.4–564.2	11–46	IC	PO	(Luo et al., 2018)
the coast of China the East China seas	2014.2015	30–40° N, 120–130° E	96.6–7238	6–48	IC	PO	(Luo et al., 2018)
Southern Ocean	2000.11	40.41° S, 144.41° E	50.4 ± 79.8	21	IC	UV	(Mace et al., 2003)
Oahu, Hawaii	1998.7.22-8.13	21.7° N, 157.8° W	46.2	31	IC	UV	(Cornell et al., 2001)
the southern margin of the East China Sea	2005-2006	25.09° N, 121.46° E	476 ± 756	24 ± 16	IC	UV with PO	(Chen and Chen, 2010)
the western North Pacific	2008.08.24-09.13	42.98° N, 144.37° E -35.65° N, 139.77° E	130 ± 61 (10–260)	67 ± 15	IC	TOC/TN analyzer	(Miyazaki et al., 2011b)
Huaniao Island	2019	30.86° N, 122.67° E	30–2810	0.13–77	IC	TOC/TN analyzer	(Tian et al., 2023)
the northern tip of Japan	2010-2012	~45.2° N, ~141.2° E	77 ± 57	12.8 ± 15.2	IC	TOC/TN analyzer	(Matsumoto et al., 2017)
the Southern Ocean	2016-2020	38.8–69.0° S, 38.1–150.8° E	4.7	20	IC	TOC/TN analyzer	(Matsumoto et al., 2022)
the Subarctic Western North Pacific Ocean	2016.7.21-8.22	30–65° N, 130–160° W	1.62–205.8	9	IC	TOC/TN analyzer	(Jung et al., 2019)
Bermuda	2011	32.27° N, 64.87° W	105 ± 191.8	50.4 ± 18.9	nutrient analyzer	TN Analyzer	(Altieri et al., 2016)
<u>the Arctic Ocean</u>	<u>2021.07-09</u> <u>2021.07-09,</u>	<u>north of ~60° N</u>	<u>5.2–32.2</u>	<u>38.6 ± 12.4</u>	<u>N Analyzer</u>	<u>N Analyzer</u>	<u>this study</u>
<u>the Coastal East Asia</u>	<u>2019.10-11,</u> <u>2023.10-2024.04</u>	<u>20–60° N</u>	<u>18.1–55.6</u>	<u>21.1 ± 7.9</u>	<u>N Analyzer</u>	<u>N Analyzer</u>	<u>this study</u>
<u>the Southwest Asia-Australia Tropical Ocean</u>	<u>2021.11, 2023.11</u>	<u>20° N-40° S</u>	<u>5.7–70.1</u>	<u>26.8 ± 10.0</u>	<u>N Analyzer</u>	<u>N Analyzer</u>	<u>this study</u>
<u>the Southern Ocean</u>	<u>2021.11-2022.03,</u> <u>2019.11, 2023.11</u>	<u>south of ~ 40° S</u>	<u>1.8–32.3</u>	<u>27.8 ± 11.0</u>	<u>N Analyzer</u>	<u>N Analyzer</u>	<u>this study</u>

*PO: the persulfate oxidation (PO) method

*UV: ultraviolet photo-oxidation

*TN analyzer: a total organic carbon (TOC) analyzer with a TN unit

*Nutrient analyzer: automated nutrient analyzer and standard colorimetric method

357 **4. Discussion**

358 **4.1 Source identification of ON**

359 ON in the MABL primarily originates from two main source pathways: marine
360 emissions and long-distance continental transport. Marine sources include primary
361 ON, predominantly associated with sea-spray particles enriched in biological material
362 from the ocean surface microlayer, and secondary ON. The latter not only derives
363 from marine precursors such as alkylamines that react with acidic species (Altieri et
364 al., 2016; Facchini et al., 2008), but also significantly involves the atmospheric
365 oxidation of marine-derived biogenic volatile organic compounds (BVOCs).
366 Specifically, isoprene and monoterpenes emitted from the ocean can react with
367 hydroxyl (OH) or nitrate radicals (NO₃) to form secondary organic nitrates (Fisher et
368 al., 2016; Ng et al., 2017). Additionally, direct sea-to-air emissions of light alkyl
369 nitrates produced photochemically in the surface water contribute to the MABL ON
370 pool (Chuck et al., 2002). Continental sources involve the long-range transport of
371 organic emissions—including combustion byproducts, soil- and vegetation-derived
372 compounds, and biomass burning aerosols. It is important to note that these
373 continental inputs include both ON formed directly over land and ON produced from
374 continental precursors during transport (Duce et al., 2008; Li et al., 2025). This
375 transport can significantly influence remote ocean regions (Cape et al., 2011; Jickells
376 et al., 2013).

377 ON concentrations in the CEA region were the highest among all study regions,
378 with air masses spending 22.6% of their 5-day trajectories over continental areas (Fig.
379 3b). A significant correlation between ON and crustal elements such as nssCa²⁺ ($r =$
380 0.75, $p < 0.01$; Fig. 4) likely suggests the influences of continental transport of
381 particles on the ON levels in this region (Xiao et al., 2016). A significant correlation
382 between ON and the anthropogenic tracer EC ($r = 0.81$, $p < 0.01$; Fig. 4) indicates that
383 fossil fuel combustion and biomass burning are important ON sources (Shubhankar
384 and Ambade, 2016; Wu and Yu, 2016). Similarly, the robust association between ON
385 and nssK⁺ ($r = 0.78$, $p < 0.01$; Fig. 4), a tracer of biomass burning, also supports
386 contributions from agricultural and residential biomass burning (Song et al., 2018).
387 Despite the high absolute ON concentrations, the relatively low ON/TN ratio (21.1%)
388 likely reflects disproportionately elevated IN emissions from intensive human
389 activities, particularly NH₃ volatilization from agriculture and vehicular NO_x

删除: , which often derives from marine precursors such as alkylamines that react with acidic species to form new particles (Altieri et al., 2016; Facchini et al., 2008)

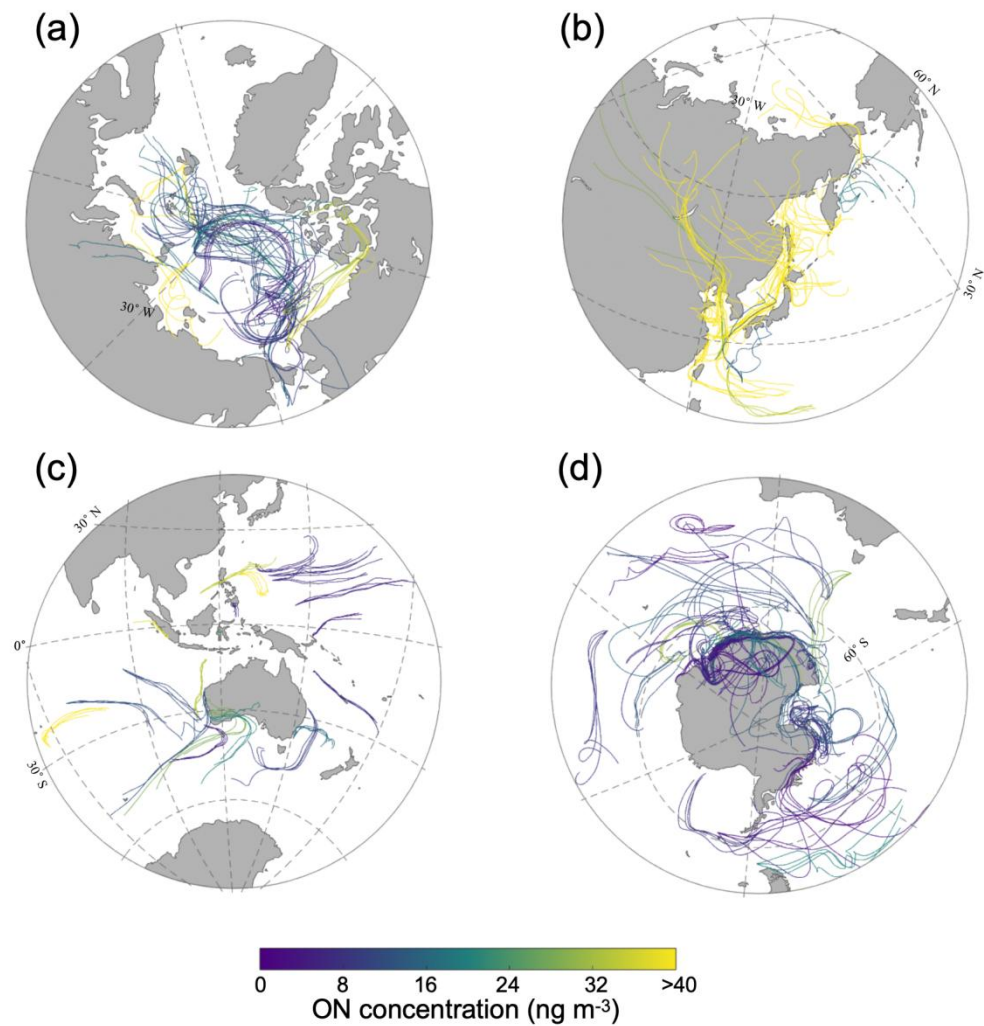
删除: —

删除: that

删除: major

390 emissions (Pavuluri et al., 2015). This interpretation aligns with emission inventories
391 that identify the CEA as a global nitrogen pollution hotspot, where ON is co-emitted
392 or formed from precursors that share common sources with EC and other
393 combustion-related pollutants, originating from incomplete combustion and industrial
394 processes (Deng et al., 2024).

395

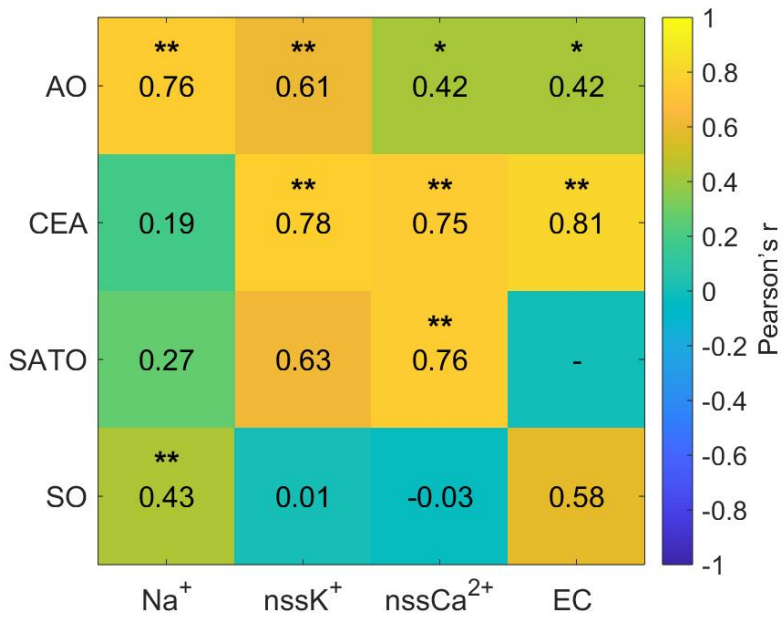


396
397 Figure 3. 5-day air-mass backward trajectories with ON concentrations and ON/TN ratios
398 along the Chinese Arctic/Antarctic expedition voyage over the Arctic Ocean (a), the coastal
399 East Asia (b), the Southeast Asia-Australia Tropical Ocean (c), and the Southern Ocean (d).

400 The SATO region exhibits intermediate level of ON concentrations (mean = 23.4
401 $\pm 18.0 \text{ ng m}^{-3}$), lower than those influenced by anthropogenic activities in CEA but
402 higher than in polar regions. In this region, ON shows a significant positive
403 correlation with nssCa^{2+} (Fig. 4; $r = 0.76, p < 0.01$), suggesting that terrestrial mineral
404 inputs (e.g., dust) influence ON levels, rather than purely marine sources. In addition,

删除: continental inputs influence ON levels

405 backward trajectory analysis showed that samples affected by continental air masses
 406 have significantly higher ON concentrations than those exposed solely to marine air
 407 (Fig. 3c), suggesting the influences of continental sources. However, ON does not
 408 exhibit significant correlations with nssK^+ or with EC ($p > 0.05$), indicating that
 409 combustion emissions may not be the primary drivers. These findings suggest that the
 410 variability of ON in the SATO region results from a mixture of marine-terrestrial
 411 interactions, primarily modulated by episodic terrestrial mineral influence rather than
 412 continuous marine emissions. Notably, this region displays an elevated ON/TN ratio
 413 (Fig. 2), primarily due to its very low IN levels—approximately 85% lower than in
 414 the CEA region—which amplifies the relative contribution of ON within TN.



415
 416 Figure 4. Spatial variations in the correlation coefficient between ON and chemical species
 417 across four regions (with “**” indicating $p < 0.01$ and “*” indicating $p < 0.05$). | 删除: ionic

418 In the AO region, ON concentrations were slightly lower than in the SATO
 419 region and significantly lower than in the CEA region. In this area, ON exhibited a
 420 significant positive correlation with Na⁺, which suggest the sea salts inputs (Fig. 4; $r =$
 421 0.43, $p < 0.01$), and also showed significant correlations with nssK⁺ ($r = 0.61$, $p <$
 422 0.01). Its correlations with nssCa²⁺ ($r = 0.42$) and EC ($r = 0.42$) were weaker but still
 423 significant ($p < 0.05$). These patterns suggest that ON in the AO region may originate
 424 not only from primary sea-salt aerosols but may also be linked to biomass burning.
 425 However, the backward trajectory analysis shows no significant difference in ON
 426 concentrations between air masses influenced by continental sources and those

427 transported solely over the ocean (Fig. S1b; independent samples t-test, $p = 0.16$),
428 likely suggesting the limited role of terrestrial inputs in this region. Unlike the SATO
429 region, where ON showed no correlation with AEC (Fig. S2b; $p > 0.05$), ON
430 concentrations in the AO exhibited a strong positive correlation with the AEC (Fig.
431 S2a; $p < 0.01$), suggesting that marine biological activity is a key driver of ON
432 variability in this region (Creamean et al., 2022). Collectively, these results
433 demonstrate that the AO region is primarily governed by marine processes, with ON
434 derived from both sea-spray organic enrichment and biogenic aerosol precursors,
435 while terrestrial influences remain secondary (Nøjgaard et al., 2022).

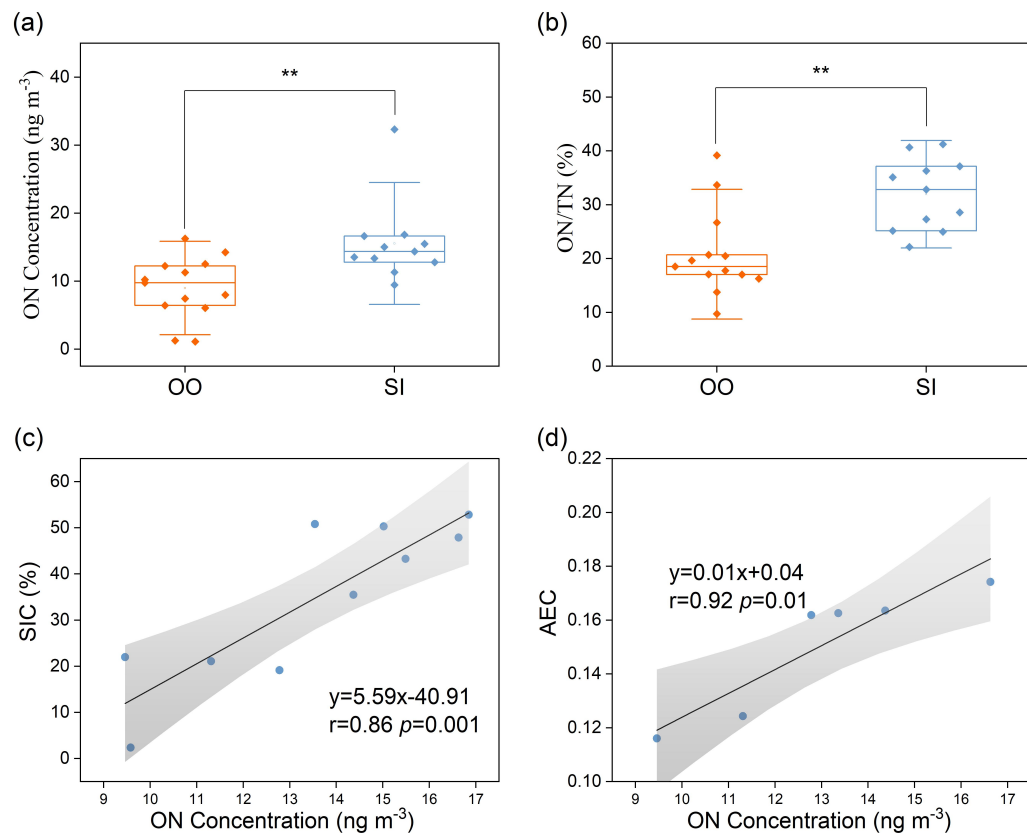
436 In the SO region, ON concentrations were the lowest among all regions (mean =
437 $12.0 \pm 7.1 \text{ ng m}^{-3}$), yet the ON/TN ratio was relatively high ($27.8 \pm 11.0\%$).
438 Back-trajectory analysis indicates that air masses predominantly originated from the
439 open ocean and Antarctic continent (Fig. 3d), with minimal anthropogenic influence.
440 ON here exhibited a significant positive correlation with Na^+ (Fig. 4; $r = 0.43$, $p <$
441 0.01), but no significant relationships with nssK^+ , nssCa^{2+} or EC. While long-range
442 transport events may deliver stable continental tracers like EC to this remote region,
443 the lack of correlation between ON and these markers suggests that continental inputs
444 are not the primary driver of ON variability. This pattern, combined with the
445 association with Na^+ suggests that primary sea-salt emissions are an important
446 pathway for ON in the SO atmosphere (Matsumoto et al., 2022), likely through the
447 incorporation of marine-derived organic matter into sea-spray aerosols. Meanwhile,
448 the absence of associations with terrestrial tracers further supports the notion that ON
449 in this remote region is likely influenced more significantly by natural marine
450 processes rather than continental or anthropogenic sources (Altieri et al., 2016). | 删除: major | 删除: controlled primarily

451 **4.2 Role of sea-ice–associated biogenic processes in shaping Antarctic aerosol ON**

452 Sea-ice and open-ocean environments create distinct conditions for the production and
453 emission of ON. While sea ice restricts direct air–sea exchange, it hosts specialized
454 microbial communities and accumulates organic matter within brine channels. During
455 melt and ice-edge retreat, this organic material is released into waters characterized by
456 high primary productivity (Arrigo et al., 2008). This biological intensification
457 enriches the surface microlayer and supplies precursors for aerosolization via sea
458 spray and secondary formation (Dall’Osto et al., 2017; DeMott et al., 2016; Galgani et
459 al., 2016; Wilson et al., 2015). | 删除: , | 删除: ing | 删除: supplying

460 Along the Antarctic coast, we classified samples into two groups based on
461 air-mass histories: open ocean (OO), influenced almost exclusively by open-ocean
462 trajectories, and sea ice (SI), with air masses residing over sea ice for extended
463 periods. SI samples exhibited significantly higher ON concentrations and ON/TN
464 ratios than OO samples ($p < 0.001$; **Mann–Whitney U test**; Fig. 5a, b). Multiple lines
465 of evidence point to sea-ice-**associated** biological processes as the driver of these
466 enhancements: (1) Strong positive correlations of ON with sea-ice concentration (SIC;
467 $r = 0.86, p < 0.01$) and with air-mass exposure to chlorophyll-a (AEC; $r = 0.91, p <$
468 0.01) in the SI group indicate that both ice cover and associated biological activity
469 elevate ON (Fig. 5c, d); (2) PSCF analysis identifies high-probability source regions
470 ($\text{PSCF} > 0.8$) over sea ice and its marginal zone for SI samples (Fig. S3c), consistent
471 with an ice-edge origin; and (3) In contrast, ON shows no significant correlation with
472 Na^+ ($r = -0.22, p > 0.05$) or with IN ($p > 0.05$) for SI samples (Fig. S4a,b), suggesting
473 that primary sea-salt emissions and purely abiotic inorganic pathways are not the
474 dominant contributors.

刪除: independent-samples t-test, $p <$
刪除: 0.01;



475
476 Figure 5. Comparison of measured ON concentrations (a) and ON/TN ratio (b) between SI
477 and OO aerosol samples (“**” indicating $p < 0.01$). And correlations between SIC (c), AEC

478 (d) and ON concentration in SI aerosol samples. The sample sizes are n = 10 for panel (c) and
479 n = 6 for panel (d). These reduced sample sizes are due to unavailable satellite SIC/Chl-a data
480 along the trajectories, and in this study SIC or Chl-a is used only when ≥ 75% of the
481 trajectory points have valid satellite values (see Sections 2.6 – 2.7).

删除: (with n = 10 and 6 for panels c and d, respectively,
owing to missing satellite data and the methodologies in
Sections 2.6 and 2.7)

482 These observations support a mechanistic pathway whereby organic matter
483 released from sympagic (ice-associated) communities during melt enriches the surface
484 microlayer and is transferred to the atmosphere via sea spray as ON-rich particles
485 (DeMott et al., 2016; Wilson et al., 2015). Concurrently, a portion of this organic
486 nitrogen is rapidly microbially degraded to volatile alkylamines (e.g., methylamines)
487 (Taubert et al., 2017), which then form aminium salts through acid–base reactions
488 with marine emissions-derived acids (e.g., H_2SO_4 , MSA), contributing to both ON
489 and IN in SI conditions (Brean et al., 2021; Dawson et al., 2012; Fitzsimons et al.,
490 2023). This process results in the formation of both organic (amine salts, contributing
491 to ON) and inorganic nitrogen aerosol species (NH_4^+ and NO_3^-), which explains their
492 elevated levels in the SI group samples (Fig. S5). The elevated ON/TN ratios in SI
493 samples (31.0%) relative to OO samples (20.8%) further indicate a greater fractional
494 contribution of ON under sea-ice influence (Fig. 5b), consistent with reported releases
495 of organic species from the sympagic ecosystem during melt (Jang et al., 2023;
496 Mirrieles et al., 2024; Yan et al., 2020).

497 For OO samples, PSCF hotspots ($\text{PSCF} > 0.8$) shift toward the offshore Southern
498 Ocean (Fig. S3d), in line with trajectories dominated by open-ocean air masses. The
499 positive association between ON and oceanic residence time ($r = 0.66$, $p < 0.01$; Fig.
500 S6) suggests that, as sea-ice influence diminishes, ON variability becomes
501 increasingly governed by open-ocean biological processes and long-range marine
502 aerosol transport.

503 Overall, these results establish the ice-edge/sympagic environment as an
504 important regulator of Antarctic aerosol ON. Sea-ice dynamics modulate both the
505 magnitude (higher ON and ON/TN) and sources (biogenic enrichment and
506 amine-driven secondary formation) of ON, underscoring the need to represent
507 sea-ice–associated processes in polar atmospheric chemistry and climate models.

508 **5. Conclusions and Implications**

509 Taking advantage of a new analytical tool for ON and aerosol samples collected from

510 three Antarctic and Arctic expeditions from 2019 to 2024, we quantified aerosol ON
511 and IN in 92 TSP samples spanning 160° of latitude in the MABL. This dataset
512 provides the first direct, subtraction-free ON measurements along a global-scale
513 marine transect, capturing both water-soluble and water-insoluble fractions.

514 We observed a pronounced hemispheric and latitudinal gradient in ON, with
515 substantially higher concentrations in the Northern Hemisphere ($83.3 \pm 141.4 \text{ ng m}^{-3}$)
516 than in the Southern Hemisphere ($15.4 \pm 12.4 \text{ ng m}^{-3}$). Regionally, Coastal East Asia
517 exhibited the highest ON ($164.6 \pm 179.1 \text{ ng m}^{-3}$) but a low ON/TN ratio (21.1%),
518 consistent with strong terrestrial and anthropogenic influences that elevate IN. The
519 Southeast Asia–Australia Tropical Ocean showed intermediate ON and a relatively
520 high ON/TN ratio due to low IN. The Arctic Ocean had lower ON but the highest
521 ON/TN ratio (38.6%), indicating prominent marine biogenic contributions. The
522 Southern Ocean showed the lowest ON ($12.0 \pm 7.0 \text{ ng m}^{-3}$) yet a relatively high
523 ON/TN ratio (27.8%), also suggestive of oceanic sources. Interannual variability
524 across the three Antarctic campaigns was minor.

525 Multiple lines of evidence, including correlations with tracers, back-trajectory
526 analysis, and PSCF, indicate that ON in CEA is dominated by continental inputs from
527 combustion and dust, whereas ON in AO and SO is primarily controlled by marine
528 processes. Along the Antarctic coast, air masses influenced by sea ice exhibited
529 significantly higher ON and ON/TN than those influenced by the open ocean, with
530 strong positive relationships to sea-ice concentration and air-mass exposure to
531 chlorophyll-a. These patterns point to sympagic and ice-edge biogenic
532 activity—through organic enrichment of sea spray and amine-driven secondary
533 formation—as key regulators of ON near Antarctica.

534 Comparison with prior WSON-only datasets suggests that earlier studies likely
535 underestimated total ON—by approximately 40% in the Southern Ocean—due to
536 omission of WION. Accounting for both soluble and insoluble phases is therefore
537 essential for constraining nitrogen deposition to the oceans and for representing ON’s
538 roles in atmospheric processes. Specifically, given that WION may significantly
539 influence cloud condensation nuclei activity and cloud droplet formation, overlooking
540 this fraction could lead to substantial uncertainties in assessing the radiative forcing
541 and climate effects of marine aerosols.

删除: aerosol–cloud interactions and radiative effects.

542 These findings fill a critical observational gap, establish robust hemispheric and
543 regional patterns of marine aerosol ON, and provide essential constraints for

544 atmospheric chemistry and climate models. Future efforts should explicitly represent
545 ON sources, including sea-ice-associated biogenic processes and amine chemistry,
546 and expand year-round, size-resolved, and composition-resolved measurements paired
547 with isotopic and molecular tracers to refine source apportionment and evaluate model
548 parameterizations across regions and seasons.

549 **Data availability.**

550 The data on organic nitrogen concentrations in aerosol are available at National
551 Tibetan Plateau/Third Pole Environment Data Center,
552 <https://cstr.cn/18406.11.Atmos.tpd.303043>. DOI:
553 <https://doi.org/10.11888/Atmos.tpd.303043> (Sun, 2025) [Dataset].

554 **Author contribution.**

555 Ningning Sun: Data curation, Writing-original draft. Yu Xu: Methodology. Bo
556 Zhang and Ye Hu: Visualization, Software. Zhe Li: Methodology. Yilan Li: Carried
557 out data analysis. Zhenlou Chen: Review. Jian Zhen Yu: Supervision, Writing –
558 review & editing. Guitao Shi: Supervision, Writing – review & editing.

559 **Competing interests.**

560 The authors declare that they have no conflict of interest.

561 **Financial support**

562 This work was supported by the National Science Foundation of China (Grant
563 Nos. 42276243 and 41922046), the Fundamental Research Funds for the Central
564 Universities, the Hong Kong Research Grants Council (1621322, 16304924 and
565 CRS_HKUST605/24)

566 **Acknowledgments**

567 The authors are grateful to CHINARE members for their support and assistance
568 in sampling. The authors acknowledge the availability of the Hybrid Single-Particle
569 Lagrangian Integrated Trajectory (HYSPLIT) model (available at
570 <https://www.arl.noaa.gov/hysplit/>)

571 **References**

572 Almeida, J., Schobesberger, S., Kürten, A., Ortega, I. K., Kupiainen-Määttä, O.,
573 Praplan, A. P., Adamov, A., Amorim, A., Bianchi, F., Breitenlechner, M., David,
574 A., Dommen, J., Donahue, N. M., Downard, A., Dunne, E., Duplissy, J., Ehrhart,
575 S., Flagan, R. C., Franchin, A., Guida, R., Hakala, J., Hansel, A., Heinritzi, M.,
576 Henschel, H., Jokinen, T., Junninen, H., Kajos, M., Kangasluoma, J., Keskinen,
577 H., Kupc, A., Kurtén, T., Kvashin, A. N., Laaksonen, A., Lehtipalo, K.,
578 Leiminger, M., Leppä, J., Loukonen, V., Makhmutov, V., Mathot, S., McGrath,
579 M. J., Nieminen, T., Olenius, T., Onnela, A., Petäjä, T., Riccobono, F., Riipinen,
580 I., Rissanen, M., Rondo, L., Ruuskanen, T., Santos, F. D., Sarnela, N., Schallhart,
581 S., Schnitzhofer, R., Seinfeld, J. H., Simon, M., Sipilä, M., Stozhkov, Y.,
582 Stratmann, F., Tomé, A., Tröstl, J., Tsagkogeorgas, G., Vaattovaara, P., Viisanen,
583 Y., Virtanen, A., Vrtala, A., Wagner, P. E., Weingartner, E., Wex, H.,
584 Williamson, C., Wimmer, D., Ye, P., Yli-Juuti, T., Carslaw, K. S., Kulmala, M.,
585 Curtius, J., Baltensperger, U., Worsnop, D. R., Vehkamäki, H., and Kirkby, J.:
586 Molecular understanding of sulphuric acid–amine particle nucleation in the
587 atmosphere, *Nature*, 502, 359–363, <https://doi.org/10.1038/nature12663>, 2013.

588 Alsante, A. N., Thornton, D. C. O., and Brooks, S. D.: Effect of Aggregation and
589 Molecular Size on the Ice Nucleation Efficiency of Proteins, *Environ. Sci.*
590 *Technol.*, 58, 4594–4605, <https://doi.org/10.1021/acs.est.3c06835>, 2024.

591 Altieri, K. E., Fawcett, S. E., Peters, A. J., Sigman, D. M., and Hastings, M. G.:
592 Marine biogenic source of atmospheric organic nitrogen in the subtropical North
593 Atlantic, *Proc. Natl. Acad. Sci. U.S.A.*, 113, 925–930,
594 <https://doi.org/10.1073/pnas.1516847113>, 2016.

595 Altieri, K. E., Fawcett, S. E., and Hastings, M. G.: Reactive Nitrogen Cycling in the
596 Atmosphere and Ocean, *Annu. Rev. Earth Planet. Sci.*, 49, 523–550,
597 <https://doi.org/10.1146/annurev-earth-083120-052147>, 2021.

598 Anonymous: A fresh look at element distribution in the North Pacific Ocean, *Eos*
599 *Trans. Am. Geophys. Union*, 78, 221–221, <https://doi.org/10.1029/97EO00148>,
600 1997.

601 Arrigo, K. R., Van Dijken, G. L., and Bushinsky, S.: Primary production in the
602 Southern Ocean, 1997–2006, *J. Geophys. Res.*, 113, 2007JC004551,
603 <https://doi.org/10.1029/2007JC004551>, 2008.

604 Ashbaugh, L. L., Malm, W. C., and Sadeh, W. Z.: A residence time probability
605 analysis of sulfur concentrations at grand Canyon National Park, *Atmos.*
606 *Environ.*, 19, 1263–1270, [https://doi.org/10.1016/0004-6981\(85\)90256-2](https://doi.org/10.1016/0004-6981(85)90256-2), 1985.

607 Baker, A. R., Kanakidou, M., Altieri, K. E., Daskalakis, N., Okin, G. S.,
608 Myriokefalitakis, S., Dentener, F., Uematsu, M., Sarin, M. M., Duce, R. A.,
609 Galloway, J. N., Keene, W. C., Singh, A., Zamora, L., Lamarque, J.-F., Hsu,
610 S.-C., Rohekar, S. S., and Prospero, J. M.: Observation- and model-based
611 estimates of particulate dry nitrogen deposition to the oceans, *Atmos. Chem.*
612 *Phys.*, 17, 8189–8210, <https://doi.org/10.5194/acp-17-8189-2017>, 2017.

613 Blazina, T., Läderach, A., Jones, G. D., Sodemann, H., Wernli, H., Kirchner, J. W.,
614 and Winkel, L. H. E.: Marine Primary Productivity as a Potential Indirect Source
615 of Selenium and Other Trace Elements in Atmospheric Deposition, *Environ. Sci.*
616 *Technol.*, 51, 108–118, <https://doi.org/10.1021/acs.est.6b03063>, 2017.

617 Brean, J., Dall’Osto, M., Simó, R., Shi, Z., Beddows, D. C. S., and Harrison, R. M.:
618 Open ocean and coastal new particle formation from sulfuric acid and amines
619 around the Antarctic Peninsula, *Nat. Geosci.*, 14, 383–388,
620 <https://doi.org/10.1038/s41561-021-00751-y>, 2021.

621 Cape, J. N., Cornell, S. E., Jickells, T. D., and Nemitz, E.: Organic nitrogen in the
622 atmosphere — Where does it come from? A review of sources and methods,
623 *Atmos. Res.*, 102, 30–48, <https://doi.org/10.1016/j.atmosres.2011.07.009>, 2011.

624 [Cavalieri, D. J., Gloersen, P., Parkinson, C. L., Comiso, J. C., and Zwally, H. J.:
625 Observed Hemispheric Asymmetry in Global Sea Ice Changes, Science, 278,
626 1104–1106, https://doi.org/10.1126/science.278.5340.1104](#), 1997.

627 Chan, M. N., Choi, M. Y., Ng, N. L., and Chan, C. K.: Hygroscopicity of
628 Water-Soluble Organic Compounds in Atmospheric Aerosols: Amino Acids and
629 Biomass Burning Derived Organic Species, *Environ. Sci. Technol.*, 39,
630 1555–1562, <https://doi.org/10.1021/es049584l>, 2005.

631 Chen, H. Y. and Chen, L.-D.: Occurrence of water soluble organic nitrogen in
632 aerosols at a coastal area, *J. Atmos. Chem.*, 65, 49–71,
633 <https://doi.org/10.1007/s10874-010-9181-y>, 2010.

634 Choi, J. H., Jang, E., Yoon, Y. J., Park, J. Y., Kim, T.-W., Becagli, S., Caiazzo, L.,
635 Cappelletti, D., Krejci, R., Eleftheriadis, K., Park, K.-T., and Jang, K. S.:
636 Influence of Biogenic Organics on the Chemical Composition of Arctic Aerosols,
637 *Global Biogeochem. Cycles*, 33, 1238–1250,

638 https://doi.org/10.1029/2019GB006226, 2019.

639 Chuck, A. L., Turner, S. M., and Liss, P. S.: Direct Evidence for a Marine Source of
640 C₁ and C₂ Alkyl Nitrates, Science, 297, 1151–1154,
641 https://doi.org/10.1126/science.1073896, 2002.

642 Cornell, S.: Water-soluble organic nitrogen in atmospheric aerosol: a comparison of
643 UV and persulfate oxidation methods, *Atmos. Environ.*, 33, 833–840,
644 https://doi.org/10.1016/S1352-2310(98)00139-3, 1999.

645 Cornell, S., Mace, K., Coeppicus, S., Duce, R., Huebert, B., Jickells, T., and Zhuang,
646 L.-Z.: Organic nitrogen in Hawaiian rain and aerosol, *J. Geophys. Res.*, 106,
647 7973–7983, https://doi.org/10.1029/2000JD900655, 2001.

648 Creamean, J. M., Barry, K., Hill, T. C. J., Hume, C., DeMott, P. J., Shupe, M. D.,
649 Dahlke, S., Willmes, S., Schmale, J., Beck, I., Hoppe, C. J. M., Fong, A.,
650 Chamberlain, E., Bowman, J., Scharien, R., and Persson, O.: Annual cycle
651 observations of aerosols capable of ice formation in central Arctic clouds, *Nat.*
652 *Commun.*, 13, 3537, https://doi.org/10.1038/s41467-022-31182-x, 2022.

653 Dall'Osto, M., Ovadnevaite, J., Paglione, M., Beddows, D. C. S., Ceburnis, D., Cree,
654 C., Cortés, P., Zamanillo, M., Nunes, S. O., Pérez, G. L., Ortega-Retuerta, E.,
655 Emelianov, M., Vaqué, D., Marrasé, C., Estrada, M., Sala, M. M., Vidal, M.,
656 Fitzsimons, M. F., Beale, R., Airs, R., Rinaldi, M., Decesari, S., Cristina
657 Facchini, M., Harrison, R. M., O'Dowd, C., and Simó, R.: Antarctic sea ice
658 region as a source of biogenic organic nitrogen in aerosols, *Sci. Rep.*, 7, 6047,
659 https://doi.org/10.1038/s41598-017-06188-x, 2017.

660 Dall'Osto, M., Airs, R. L., Beale, R., Cree, C., Fitzsimons, M. F., Beddows, D.,
661 Harrison, R. M., Ceburnis, D., O'Dowd, C., Rinaldi, M., Paglione, M., Nenes, A.,
662 Decesari, S., and Simó, R.: Simultaneous Detection of Alkylamines in the
663 Surface Ocean and Atmosphere of the Antarctic Sympagic Environment, *ACS*
664 *Earth Space Chem.*, 3, 854–862,
665 https://doi.org/10.1021/acsearthspacechem.9b00028, 2019.

666 Dawson, M. L., Varner, M. E., Perraud, V., Ezell, M. J., Gerber, R. B., and
667 Finlayson-Pitts, B. J.: Simplified mechanism for new particle formation from
668 methanesulfonic acid, amines, and water via experiments and ab initio
669 calculations, *Proc. Natl. Acad. Sci. U.S.A.*, 109, 18719–18724,
670 https://doi.org/10.1073/pnas.1211878109, 2012.

671 DeMott, P. J., Hill, T. C. J., McCluskey, C. S., Prather, K. A., Collins, D. B., Sullivan,

672 R. C., Ruppel, M. J., Mason, R. H., Irish, V. E., Lee, T., Hwang, C. Y., Rhee, T.
673 S., Snider, J. R., McMeeking, G. R., Dhaniyala, S., Lewis, E. R., Wentzell, J. J.
674 B., Abbatt, J., Lee, C., Sultana, C. M., Ault, A. P., Axson, J. L., Diaz Martinez,
675 M., Venero, I., Santos-Figueroa, G., Stokes, M. D., Deane, G. B., Mayol-Bracero,
676 O. L., Grassian, V. H., Bertram, T. H., Bertram, A. K., Moffett, B. F., and Franc,
677 G. D.: Sea spray aerosol as a unique source of ice nucleating particles, Proc. Natl.
678 Acad. Sci. U.S.A., 113, 5797–5803, <https://doi.org/10.1073/pnas.1514034112>,
679 2016.

680 Deng, O., Wang, S., Ran, J., Huang, S., Zhang, X., Duan, J., Zhang, L., Xia, Y., Reis,
681 S., Xu, J., Xu, J., De Vries, W., Sutton, M. A., and Gu, B.: Managing urban
682 development could halve nitrogen pollution in China, Nat. Commun., 15, 401,
683 <https://doi.org/10.1038/s41467-023-44685-y>, 2024.

684 [Duce, R. A., LaRoche, J., Altieri, K., Arrigo, K. R., Baker, A. R., Capone, D. G.,](#)
685 [Cornell, S., Dentener, F., Galloway, J., Ganeshram, R. S., Geider, R. J., Jickells,](#)
686 [T., Kuypers, M. M., Langlois, R., Liss, P. S., Liu, S. M., Middelburg, J. J.,](#)
687 [Moore, C. M., Nickovic, S., Oschlies, A., Pedersen, T., Prospero, J., Schlitzer, R.,](#)
688 [Seitzinger, S., Sorensen, L. L., Uematsu, M., Ulloa, O., Voss, M., Ward, B., and](#)
689 [Zamora, L.: Impacts of Atmospheric Anthropogenic Nitrogen on the Open](#)
690 [Ocean, Science, 320, 893–897, https://doi.org/10.1126/science.1150369, 2008.](#)

691 Facchini, M. C., Decesari, S., Rinaldi, M., Carbone, C., Finessi, E., Mircea, M., Fuzzi,
692 S., Moretti, F., Tagliavini, E., Ceburnis, D., and O'Dowd, C. D.: Important
693 Source of Marine Secondary Organic Aerosol from Biogenic Amines, Environ.
694 Sci. Technol., 42, 9116–9121, <https://doi.org/10.1021/es8018385>, 2008.

695 [Fetterer, F., Knowles, K., Meier, W. N., Savoie, M. and Windnagel, A. K.: Sea Ice](#)
696 [Index. \(G02135, Version 3\). \[Data Set\]. Boulder, Colorado USA. National Snow](#)
697 [and Ice Data Center. https://doi.org/10.7265/N5K072F8, 2017.](#)

698 [Fisher, J. A., Jacob, D. J., Travis, K. R., Kim, P. S., Marais, E. A., Chan Miller, C., Yu,](#)
699 [K., Zhu, L., Yantosca, R. M., Sulprizio, M. P., Mao, J., Wennberg, P. O., Crounse,](#)
700 [J. D., Teng, A. P., Nguyen, T. B., St. Clair, J. M., Cohen, R. C., Romer, P., Nault,](#)
701 [B. A., Wooldridge, P. J., Jimenez, J. L., Campuzano-Jost, P., Day, D. A., Hu, W.,](#)
702 [Shepson, P. B., Xiong, F., Blake, D. R., Goldstein, A. H., Misztal, P. K., Hanisco,](#)
703 [T. F., Wolfe, G. M., Ryerson, T. B., Wisthaler, A., and Mikoviny, T.: Organic](#)
704 [nitrate chemistry and its implications for nitrogen budgets in an isoprene- and](#)
705 [monoterpene-rich atmosphere: constraints from aircraft \(SEAC⁴ RS\) and](#)

706 [ground-based \(SOAS\) observations in the Southeast US, Atmos. Chem. Phys., 16, 5969–5991, https://doi.org/10.5194/acp-16-5969-2016, 2016.](https://doi.org/10.5194/acp-16-5969-2016, 2016)

707

708 Fitzsimons, M. F., Tilley, M., and Cree, C. H. L.: The determination of volatile
709 amines in aquatic marine systems: A review, *Anal. Chim. Acta*, 1241, 340707,
710 <https://doi.org/10.1016/j.aca.2022.340707>, 2023.

711 Galgani, L., Piontek, J., and Engel, A.: Biopolymers form a gelatinous microlayer at
712 the air-sea interface when Arctic sea ice melts, *Sci. Rep.*, 6, 29465,
713 <https://doi.org/10.1038/srep29465>, 2016.

714 Jang, J., Park, J., Park, J., Yoon, Y. J., Dall'Osto, M., Park, K.-T., Jang, E., Lee, J. Y.,
715 Cho, K. H., and Lee, B. Y.: Ocean-atmosphere interactions: Different organic
716 components across Pacific and Southern Oceans, *Sci. Total Environ.*, 878,
717 162969, <https://doi.org/10.1016/j.scitotenv.2023.162969>, 2023.

718 Jickells, T., Baker, A. R., Cape, J. N., Cornell, S. E., and Nemitz, E.: The cycling of
719 organic nitrogen through the atmosphere, *Phil. Trans. R. Soc. B*, 368, 20130115,
720 <https://doi.org/10.1098/rstb.2013.0115>, 2013.

721 Jung, J., Han, B., Rodriguez, B., Miyazaki, Y., Chung, H. Y., Kim, K., Choi, J.-O.,
722 Park, K., Kim, I.-N., Kim, S., Yang, E. J., and Kang, S.-H.: Atmospheric Dry
723 Deposition of Water-Soluble Nitrogen to the Subarctic Western North Pacific
724 Ocean during Summer, *Atmosphere*, 10, 351,
725 <https://doi.org/10.3390/atmos10070351>, 2019.

726 Keene, W. C., Pszenny, A. A. P., Galloway, J. N., and Hawley, M. E.: Sea-salt
727 corrections and interpretation of constituent ratios in marine precipitation, *J.*
728 *Geophys. Res.*, 91, 6647–6658, <https://doi.org/10.1029/JD091iD06p06647>, 1986.

729 Lesworth, T., Baker, A. R., and Jickells, T.: Aerosol organic nitrogen over the remote
730 Atlantic Ocean, *Atmos. Environ.*, 44, 1887–1893,
731 <https://doi.org/10.1016/j.atmosenv.2010.02.021>, 2010.

732 Li, Y., Fu, T.-M., Yu, J. Z., Yu, X., Chen, Q., Miao, R., Zhou, Y., Zhang, A., Ye, J.,
733 Yang, X., Tao, S., Liu, H., and Yao, W.: Dissecting the contributions of organic
734 nitrogen aerosols to global atmospheric nitrogen deposition and implications for
735 ecosystems, *Natl. Sci. Rev.*, 10, nwad244, <https://doi.org/10.1093/nsr/nwad244>,
736 2023.

737 Li, Y., Fu, T.-M., Yu, J. Z., Zhang, A., Yu, X., Ye, J., Zhu, L., Shen, H., Wang, C.,
738 Yang, X., Tao, S., Chen, Q., Li, Y., Li, L., Che, H., and Heald, C. L.: Nitrogen
739 dominates global atmospheric organic aerosol absorption, *Science*, 387, 989–995,

740 https://doi.org/10.1126/science.adr4473, 2025.

741 Luo, L., Kao, S.-J., Bao, H., Xiao, H., Xiao, H., Yao, X., Gao, H., Li, J., and Lu, Y.:
742 Sources of reactive nitrogen in marine aerosol over the Northwest Pacific Ocean
743 in spring, *Atmos. Chem. Phys.*, 18, 6207–6222,
744 https://doi.org/10.5194/acp-18-6207-2018, 2018.

745 Mace, K. A., Duce, R. A., and Tindale, N. W.: Organic nitrogen in rain and aerosol at
746 Cape Grim, Tasmania, Australia, *J. Geophys. Res.*, 108, 2002JD003051,
747 https://doi.org/10.1029/2002JD003051, 2003.

748 Matsumoto, K., Yamamoto, Y., Nishizawa, K., Kaneyasu, N., Irino, T., and
749 Yoshikawa-Inoue, H.: Origin of the water-soluble organic nitrogen in the
750 maritime aerosol, *Atmos. Environ.*, 167, 97–103,
751 https://doi.org/10.1016/j.atmosenv.2017.07.050, 2017.

752 Matsumoto, K., Kobayashi, H., Hara, K., Ishino, S., and Hayashi, M.: Water-soluble
753 organic nitrogen in fine aerosols over the Southern Ocean, *Atmos. Environ.*, 287,
754 119287, https://doi.org/10.1016/j.atmosenv.2022.119287, 2022.

755 Mirrielees, J. A., Kirpes, R. M., Costa, E. J., Porter, G. C. E., Murray, B. J., Lata, N.
756 N., Boschi, V., China, S., Grannas, A. M., Ault, A. P., Matrai, P. A., and Pratt, K.
757 A.: Marine aerosol generation experiments in the High Arctic during
758 summertime, *Elem Sci Anth*, 12, 00134,
759 https://doi.org/10.1525/elementa.2023.00134, 2024.

760 Miyazaki, Y., Kawamura, K., Jung, J., Furutani, H., and Uematsu, M.: Latitudinal
761 distributions of organic nitrogen and organic carbon in marine aerosols over the
762 western North Pacific, *Atmos. Chem. Phys.*, 11, 3037–3049,
763 https://doi.org/10.5194/acp-11-3037-2011, 2011a.

764 Miyazaki, Y., Kawamura, K., Jung, J., Furutani, H., and Uematsu, M.: Latitudinal
765 distributions of organic nitrogen and organic carbon in marine aerosols over the
766 western North Pacific, *Atmos. Chem. Phys.*, 11, 3037–3049,
767 https://doi.org/10.5194/acp-11-3037-2011, 2011b.

768 Ng, N. L., Brown, S. S., Archibald, A. T., Atlas, E., Cohen, R. C., Crowley, J. N., Day,
769 D. A., Donahue, N. M., Fry, J. L., Fuchs, H., Griffin, R. J., Guzman, M. I.,
770 Herrmann, H., Hodzic, A., Iinuma, Y., Jimenez, J. L., Kiendler-Scharr, A., Lee,
771 B. H., Luecken, D. J., Mao, J., McLaren, R., Mutzel, A., Osthoff, H. D., Ouyang,
772 B., Picquet-Varrault, B., Platt, U., Pye, H. O. T., Rudich, Y., Schwantes, R. H.,
773 Shiraiwa, M., Stutz, J., Thornton, J. A., Tilgner, A., Williams, B. J., and Zaveri,

774 [R. A.: Nitrate radicals and biogenic volatile organic compounds: oxidation,](https://doi.org/10.5194/acp-17-2103-2017, 2017)
775 [mechanisms, and organic aerosol, Atmos. Chem. Phys., 17, 2103–2162,](https://doi.org/10.5194/acp-17-2103-2017, 2017)
776 [https://doi.org/10.5194/acp-17-2103-2017, 2017.](https://doi.org/10.5194/acp-17-2103-2017, 2017)

777 Nøjgaard, J. K., Peker, L., Pernov, J. B., Johnson, M. S., Bossi, R., Massling, A.,
778 Lange, R., Nielsen, I. E., Prevot, A. S. H., Eriksson, A. C., Canonaco, F., and
779 Skov, H.: A local marine source of atmospheric particles in the High Arctic,
780 *Atmos. Environ.*, 285, 119241, <https://doi.org/10.1016/j.atmosenv.2022.119241>,
781 2022.

782 [Park, K., Lee, K., Kim, T., Yoon, Y. J., Jang, E., Jang, S., Lee, B., and Hermansen, O.: Atmospheric DMS in the Arctic Ocean and Its Relation to Phytoplankton](https://doi.org/10.1002/2017GB005805, 2018)
783 [Biomass, Global Biogeochem. Cycles, 32, 351–359,](https://doi.org/10.1002/2017GB005805, 2018)
784 [https://doi.org/10.1002/2017GB005805, 2018.](https://doi.org/10.1002/2017GB005805, 2018)

785 Pavuluri, C. M., Kawamura, K., and Fu, P. Q.: Atmospheric chemistry of nitrogenous
786 aerosols in northeastern Asia: biological sources and secondary formation,
787 *Atmos. Chem. Phys.*, 15, 9883–9896, <https://doi.org/10.5194/acp-15-9883-2015>,
788 2015.

789 Quinby-Hunt, M. S. and Turehian, K. K.: Distribution of elements in sea water, *EoS*
790 *Trans. Am. Geophys. Union*, 64, 130–130,
791 [https://doi.org/10.1029/EO064i014p00130, 1983.](https://doi.org/10.1029/EO064i014p00130, 1983)

792 Shi, G., Ma, H., Zhu, Z., Hu, Z., Chen, Z., Jiang, S., An, C., Yu, J., Ma, T., Li, Y.,
793 Sun, B., and Hastings, M. G.: Using stable isotopes to distinguish atmospheric
794 nitrate production and its contribution to the surface ocean across hemispheres,
795 *Earth Planet. Sci. Lett.*, 564, 116914, <https://doi.org/10.1016/j.epsl.2021.116914>,
796 2021.

797 Shubhankar, B. and Ambade, B.: Chemical characterization of carbonaceous carbon
798 from industrial and semi urban site of eastern India, *SpringerPlus*, 5, 837,
799 [https://doi.org/10.1186/s40064-016-2506-9, 2016.](https://doi.org/10.1186/s40064-016-2506-9, 2016)

800 Siegel, D. A., Behrenfeld, M. J., Maritorena, S., McClain, C. R., Antoine, D., Bailey,
801 S. W., Bontempi, P. S., Boss, E. S., Dierssen, H. M., Doney, S. C., Eplee, R. E.,
802 Evans, R. H., Feldman, G. C., Fields, E., Franz, B. A., Kuring, N. A., Mengelt,
803 C., Nelson, N. B., Patt, F. S., Robinson, W. D., Sarmiento, J. L., Swan, C. M.,
804 Werdell, P. J., Westberry, T. K., Wilding, J. G., and Yoder, J. A.: Regional to
805 global assessments of phytoplankton dynamics from the SeaWiFS mission,
806 *Remote Sens. Environ.*, 135, 77–91, <https://doi.org/10.1016/j.rse.2013.03.025>,

808 2013.

809 Song, J., Zhao, Y., Zhang, Y., Fu, P., Zheng, L., Yuan, Q., Wang, S., Huang, X., Xu,
810 W., Cao, Z., Gromov, S., and Lai, S.: Influence of biomass burning on
811 atmospheric aerosols over the western South China Sea: Insights from ions,
812 carbonaceous fractions and stable carbon isotope ratios, *Environ. Pollut.*, 242,
813 1800–1809, <https://doi.org/10.1016/j.envpol.2018.07.088>, 2018.

814 Stein, A. F., Draxler, R. R., Rolph, G. D., Stunder, B. J. B., Cohen, M. D., and Ngan,
815 F.: NOAA's HYSPLIT Atmospheric Transport and Dispersion Modeling System,
816 *Bull. Am. Meteorol. Soc.*, 96, 2059–2077,
817 <https://doi.org/10.1175/BAMS-D-14-00110.1>, 2015.

818 Sun, N.: Spatial distribution of organic nitrogen in the global marine boundary layer
819 from Arctic to Antarctic, National Tibetan Plateau / Third Pole Environment
820 Data Center), <https://doi.org/10.11888/Atmos.tpd.303043>, 2025.

821 Taubert, M., Grob, C., Howat, A. M., Burns, O. J., Pratscher, J., Jehmlich, N., Von
822 Bergen, M., Richnow, H. H., Chen, Y., and Murrell, J. C.: Methylamine as a
823 nitrogen source for microorganisms from a coastal marine environment, *Environ.*
824 *Microbiol.*, 19, 2246–2257, <https://doi.org/10.1111/1462-2920.13709>, 2017.

825 Tian, M., Li, H., Wang, G., Fu, M., Qin, X., Lu, D., Liu, C., Zhu, Y., Luo, X., Deng,
826 C., Abdullaev, S. F., and Huang, K.: Seasonal source identification and
827 formation processes of marine particulate water soluble organic nitrogen over an
828 offshore island in the East China Sea, *Sci. Total Environ.*, 863, 160895,
829 <https://doi.org/10.1016/j.scitotenv.2022.160895>, 2023.

830 Violaki, K., Sciare, J., Williams, J., Baker, A. R., Martino, M., and Mihalopoulos, N.:
831 Atmospheric water-soluble organic nitrogen (WSON) over marine environments:
832 a global perspective, *Biogeosciences*, 12, 3131–3140,
833 <https://doi.org/10.5194/bg-12-3131-2015>, 2015a.

834 Violaki, K., Sciare, J., Williams, J., Baker, A. R., Martino, M., and Mihalopoulos, N.:
835 Atmospheric water-soluble organic nitrogen (WSON) over marine environments:
836 a global perspective, *Biogeosciences*, 12, 3131–3140,
837 <https://doi.org/10.5194/bg-12-3131-2015>, 2015b.

838 Wilson, T. W., Ladino, L. A., Alpert, P. A., Breckels, M. N., Brooks, I. M., Browse, J.,
839 Burrows, S. M., Carslaw, K. S., Huffman, J. A., Judd, C., Kilthau, W. P., Mason,
840 R. H., McFiggans, G., Miller, L. A., Nájera, J. J., Polishchuk, E., Rae, S.,
841 Schiller, C. L., Si, M., Temprado, J. V., Whale, T. F., Wong, J. P. S., Wurl, O.,

842 Yakobi-Hancock, J. D., Abbatt, J. P. D., Aller, J. Y., Bertram, A. K., Knopf, D.
843 A., and Murray, B. J.: A marine biogenic source of atmospheric ice-nucleating
844 particles, *Nature*, 525, 234–238, <https://doi.org/10.1038/nature14986>, 2015.

845 Wu, C. and Yu, J. Z.: Determination of primary combustion source organic
846 carbon-to-elemental carbon (OC / EC) ratio using ambient OC and EC
847 measurements: secondary OC-EC correlation minimization method, *Atmos.*
848 *Chem. Phys.*, 16, 5453–5465, <https://doi.org/10.5194/acp-16-5453-2016>, 2016.

849 Wu, G., Hu, Y., Gong, C., Wang, D., Zhang, F., Herath, I. K., Chen, Z., and Shi, G.:
850 Spatial distribution, sources, and direct radiative effect of carbonaceous aerosol
851 along a transect from the Arctic Ocean to Antarctica, *Sci. Total Environ.*, 916,
852 170136, <https://doi.org/10.1016/j.scitotenv.2024.170136>, 2024.

853 Xiao, H.-W., Xiao, H.-Y., Luo, L., Shen, C.-Y., Long, A.-M., Chen, L., Long, Z.-H.,
854 and Li, D.-N.: Atmospheric aerosol compositions over the South China Sea:
855 temporal variability and source apportionment, *Atmos. Chem. Phys.*, 17,
856 3199–3214, <https://doi.org/10.5194/acp-17-3199-2017>, 2017.

857 Yan, J., Jung, J., Lin, Q., Zhang, M., Xu, S., and Zhao, S.: Effect of sea ice retreat on
858 marine aerosol emissions in the Southern Ocean, Antarctica, *Sci. Total Environ.*,
859 745, 140773, <https://doi.org/10.1016/j.scitotenv.2020.140773>, 2020.

860 Yan, S., Xu, G., Zhang, H., Wang, J., Xu, F., Gao, X., Zhang, J., Wu, J., and Yang, G.:
861 Factors Controlling DMS Emission and Atmospheric Sulfate Aerosols in the
862 Western Pacific Continental Sea, *J. Geophys. Res.*, 129, e2024JC020886,
863 <https://doi.org/10.1029/2024JC020886>, 2024.

864 Yu, X., Li, Q., Ge, Y., Li, Y., Liao, K., Huang, X. H., Li, J., and Yu, J. Z.:
865 Simultaneous Determination of Aerosol Inorganic and Organic Nitrogen by
866 Thermal Evolution and Chemiluminescence Detection, *Environ. Sci. Technol.*,
867 55, 11579–11589, <https://doi.org/10.1021/acs.est.1c04876>, 2021.

868 Zamora, L. M., Prospero, J. M., and Hansell, D. A.: Organic nitrogen in aerosols and
869 precipitation at Barbados and Miami: Implications regarding sources, transport
870 and deposition to the western subtropical North Atlantic, *J. Geophys. Res.*, 116,
871 D20309, <https://doi.org/10.1029/2011JD015660>, 2011.

872 Zhou, S., Chen, Y., Paytan, A., Li, H., Wang, F., Zhu, Y., Yang, T., Zhang, Y., and
873 Zhang, R.: Non-Marine Sources Contribute to Aerosol Methanesulfonate Over
874 Coastal Seas, JGR Atmospheres, 126, e2021JD034960,
875 <https://doi.org/10.1029/2021JD034960>, 2021.

876 Zhou, S., Chen, Y., Wang, F., Bao, Y., Ding, X., and Xu, Z.: Assessing the Intensity
877 of Marine Biogenic Influence on the Lower Atmosphere: An Insight into the
878 Distribution of Marine Biogenic Aerosols over the Eastern China Seas, Environ.
879 Sci. Technol., 57, 12741–12751, <https://doi.org/10.1021/acs.est.3c04382>, 2023.